Chinese Chemical Letters 32 (2021) 3501–3504

Contents lists available at ScienceDirect

Chinese Chemical Letters

journal homepage: www.elsevier.com/locate/cclet

Communication

The metallic 1T-WS_2 as cocatalysts for promoting photocatalytic N_2 fixation performance of Bi_5O_7Br nanosheets

Pengyuan Qiu[a], Jianwei Wang[a], Zhangqian Liang[a], Yanjun Xue[a], Yanli Zhou[b], Xiaoli Zhang[c], Hongzhi Cui[a,*], Guiqing Cheng[a,*], Jian Tian[a,*]

[a] School of Materials Science and Engineering, Shandong University of Science and Technology, Qingdao 266590, China
[b] School of Environmental and Material Engineering, Yantai University, Yantai 264005, China
[c] School of Materials Science and Engineering, Zhengzhou University, Zhengzhou 450001, China

ARTICLE INFO

Article history:
Received 23 February 2021
Received in revised form 26 March 2021
Accepted 29 March 2021
Available online 31 March 2021

Keywords:
Photocatalytic N_2 fixation
Bi_5O_7Br
1T phase WS_2
Electron-hole pairs
Photocatalytic performance

ABSTRACT

Recently, widespread attention has been devoted to the typical layered BiOCl or BiOBr because of the suitable nanostructure and band structure. However, owing to the fast carrier recombination, the photocatalytic performance of BiOX materials is not so satisfactory. Loading 1T phase WS_2 nanosheets (NSs) onto Bi_5O_7Br NSs can improve the photocatalytic N_2 fixation activity. Among these, the obtained 1T-WS_2@Bi_5O_7Br composites with optimum 5% 1T-WS_2 NSs display a significantly improved photocatalytic N_2 fixation rate (8.43 mmol L^{-1} h^{-1} g^{-1}), 2.51 times higher than pure Bi_5O_7Br (3.36 mmol L^{-1} h^{-1} g^{-1}). And the outstanding stability of 1T-WS_2@Bi_5O_7Br-5 composites is also achieved. Exactly, the photoexcited electrons from Bi_5O_7Br NSs are quickly transferred to conductive 1T phase WS_2 as electron acceptors, which can promote the separation of carriers. In addition, 1T-WS_2 NSs can provide abundant active sites on the basal and edge planes, which can promote the efficiency of photocatalytic N_2 fixation. This work offers a novel solution to improve the photocatalytic performance of Bi_5O_7Br NSs.

Ammonia (NH_3) is one of the most significant raw materials for agriculture and industry [1]. The synthesis method of NH_3 usually uses the high pressure and temperature Haber-Bosch method [2–4]. Schrauzer *et al.* first invented that N_2 could be photo-reduced to form NH_3 on Fe-doped TiO_2 in 1977 [5]. This approach uses H_2O and N_2 as raw materials and renewable solar energy as an energy source, which not only greatly reduces the cost of raw materials, but also saves energy. Therefore, photocatalytic technology is recognized as the most promising way to replace Haber-Bosch method [6]. However, photocatalytic N_2 fixation is still an enormous challenge due to the solid N≡N bond and the weak N_2 adsorption on photocatalyst [7,8]. Therefore, it is particularly vital to seek a high-performance photocatalyst.

Recent studies have shown that typical layered BiOCl and BiOBr display outstanding photocatalytic performance attributing to the suitable nanostructure and band structure [9–13]. For example, Liu *et al.* have studied Bi_5O_7Br, which has abundant oxygen vacancies (OVs) and the OVs can enhance the photocatalytic N_2 activation of O-terminated+H facets [14]. Another research has shown that BiOX-based semiconductors can adsorb and activate N_2 well owning to OVs with abundant localized electrons on the surface [15–18]. Therefore, Bi_5O_7Br rich in inherent oxygen vacancies can be applied to photocatalytic nitrogen fixation. However, the photocatalytic activity of pure Bi_5O_7Br is limited due to the fast carrier recombination. Appropriate cocatalyst modification of photocatalyst is an efficient way for greatly enhancing photocatalytic performance and stability, due to the lower activation potential for the N_2 fixation reaction and efficient separation of photogenerated charges [19–21]. Most of the cocatalysts are precious metals, such as Pt [22]. However, the widespread use of precious metals is greatly confined by their scarcities and high prices, so it is essential to develop earth-rich and cheap cocatalysts [22–24].

Transition-metal chalcogenides, such as WS_2, receive widespread attention due to the superior 2D layered structure [25–28]. WS_2 possesses both metallic 1T phase and semiconductor 2H phase. It has been confirmed that 1T phase WS_2 with octahedral coordination can promote the capture and transfer of carriers to improve the photocatalytic performance, attributing to excellent conductivity [28]. Although 1T phase WS_2 as cocatalysts has been studied, the research on 1T-WS_2 to improve the photocatalytic activity of Bi_5O_7Br has not been reported.

* Corresponding authors.
E-mail addresses: cuihongzhi1965@163.com (H. Cui), chengguiqing@sdust.edu.cn (G. Cheng), jiantian@sdust.edu.cn (J. Tian).

https://doi.org/10.1016/j.cclet.2021.03.077
1001-8417/

In this research work, the 1T phase WS_2 NSs decorated Bi_5O_7Br NSs (named 1T-WS_2@Bi_5O_7Br composites) have narrower band gap, more effective carrier transport efficiency and better light absorption ability. After testing, 1T-WS_2@Bi_5O_7Br-5 composites present the best photocatalytic nitrogen fixation performance (8.43 mmol L^{-1} h^{-1} g^{-1}) and excellent stability. The probable photocatalytic mechanism of 1T-WS_2@Bi_5O_7Br composites is proposed.

The Bi_5O_7Br NSs were prepared by a self-assembly water-induced process (Scheme 1a). Firstly, ammonia solution and bismuth(III) nitrate pentahydrate were added into a beaker, and then potassium bromide was added into a beaker. Finally, the mixtures were heated at 40 °C to obtain Bi_5O_7Br NSs with rich oxygen vacancies. As shown in Scheme 1b, the metallic 1T-WS_2 NSs were prepared via a solvothermal process. Tungsten(VI) chloride and TAA were dissolved in DMF, and then the mixed solution was hydrothermally heated at 200 °C for 24 h to obtain 1T-WS_2 NSs. The 1T-WS_2@Bi_5O_7Br composites were synthesized by an ordinary grinding process (Scheme 1c). Bi_5O_7Br NSs and 1T-WS_2 NSs were added in a mortar with ethanol and hexane to fully grind. The mixed powder was dried to obtain 1T-WS_2@Bi_5O_7Br composites.

For pure Bi_5O_7Br NSs, three typical diffraction peaks are located at 2θ of 29.3°, 32.64° and 56.62° (green curve in Fig. 1a), attributing to (113), (600) and (912) planes of tetragonal Bi_5O_7Br (JCPDS card No. 038-0493) [29,30]. This illustrates the successful preparation of tetragonal Bi_5O_7Br. The XRD patterns of 1T-WS_2@Bi_5O_7Br composites are similar to that of pure Bi_5O_7Br NSs, indicating that the size and structure of Bi_5O_7Br are not destroyed [31]. In addition, with the increased loading of 1T-WS_2 from 1% to 7%, the characteristic peaks of Bi_5O_7Br become weaker, which shows that the 1T-WS_2 loading reduces the order degree of Bi_5O_7Br [32]. For pure 1T-WS_2 NSs (black curve in Fig. 1a), two obvious peaks located at 2θ of 9.3° (002) and 18.3° (004) indicate the successful preparation of metallic 1T-WS_2 [33]. However, no diffraction peak of 1T-WS_2 is found in the XRD pattern of 1T-WS_2@Bi_5O_7Br composites, which is attributed to the low 1T-WS_2 loading amount.

The survey scan of 1T-WS_2@Bi_5O_7Br composites (Fig. S1a in Supporting information) confirms that it consists of Bi, O, Br, S and W. The Bi 4f XPS spectrum (Fig. S1b in Supporting information) could be deconvoluted into two main peaks at 163.9 and 158.5 eV, corresponding to the $4f_{5/2}$ and $4f_{7/2}$ of Bi^{3+} [30]. From Fig. S1c (Supporting information), there are three peaks of O 1s XPS spectrum at 529.4, 530.2 and 531.3 eV, attributing to the lattice

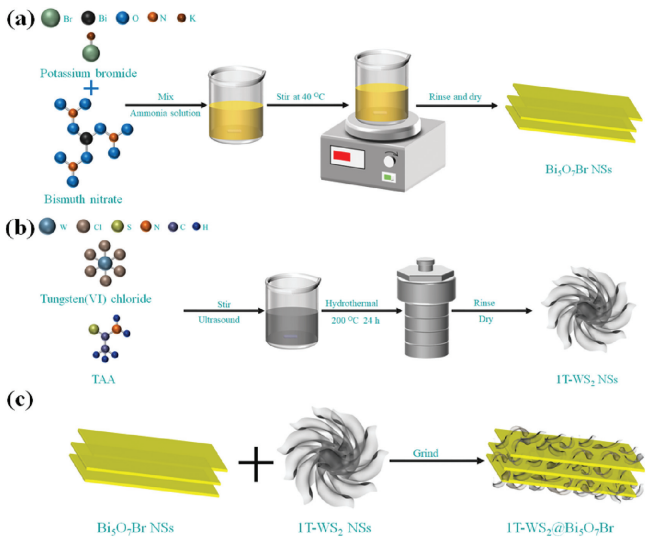

Scheme 1. The schematic synthetic route diagram of (a) pure Bi_5O_7Br NSs, (b) 1T-WS_2 NSs and (c) 1T-WS_2@Bi_5O_7Br composites.

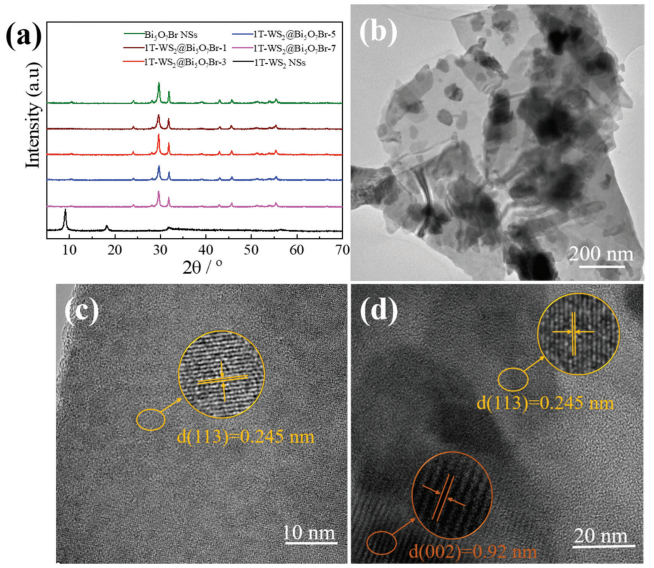

Fig. 1. (a) XRD patterns of pure Bi_5O_7Br NSs, 1T-WS_2 NSs and 1T-WS_2@Bi_5O_7Br composites. (b) TEM images of 1T-WS_2@Bi_5O_7Br-5 composites. HR-TEM images of (c) Bi_5O_7Br and (d) 1T-WS_2@Bi_5O_7Br-5 composites.

oxygen, oxygen vacancies and absorbed oxygen, further confirming the existence of oxygen vacancies in the 1T-WS_2@Bi_5O_7Br composites [29]. For the XPS spectrum of Br 3d (Fig. S1d in Supporting information), two main peaks at 67.8 and 68.9 eV are attributed to the $3d_{5/2}$ and $3d_{3/2}$ of Br^- [30]. The XPS spectra of S 2p and W 4f are investigated to prove the existence of 1T phase WS_2 (Figs. S1e and f in Supporting information). For the S 2p spectrum (Fig. S1e), two main peaks at 161.7 and 162.9 eV corresponds to S $2p_{3/2}$ and S $2p_{1/2}$ of 1T-WS_2 [33]. Besides, two small peaks at 163.5 and 164.7 eV own to S $2p_{3/2}$ and S $2p_{1/2}$ of 2H-WS_2 [33]. As shown in Fig. S1f, there are two visible peaks at 31.9 and 34.1 eV, attributing to W $4f_{7/2}$ and W $4f_{5/2}$ of 1T-WS_2 [27]. The two minor peaks at 32.9 (W $4f_{7/2}$) and 35.6 eV (W $4f_{5/2}$) correlate to 2H-WS_2, respectively. After deconvoluting W 4f and S 2p spectra, the proportion of 1T phase is about 66.2%, which indicates that 1T phase in 1T-WS_2@Bi_5O_7Br-5 composites is the main phase.

The structure of as-prepared pure 1T-WS_2 NSs is observed by SEM (Fig. S2 in Supporting information). Pure 1T-WS_2 presents the flower-like assemblies with nanosheets. The morphologies and microstructures information of pure Bi_5O_7Br and 1T-WS_2@Bi_5O_7Br-5 composites are provided by TEM and HRTEM. As shown in Fig. S3 (Supporting information), pure Bi_5O_7Br NSs display the compact lamellar structure. And 1T-WS_2@Bi_5O_7Br-5 composites also maintain the sheet-shaped morphology of pure Bi_5O_7Br (Fig. 1b). In addition, numerous small 1T-WS_2 NSs are intimately loaded on the surface of 1T-WS_2@Bi_5O_7Br-5 composites. As displayed in Fig. S4, Bi, O, Br, S and W elements are uniformly distributed on 1T-WS_2@Bi_5O_7Br-5 composites, which further confirms that numerous 1T-WS_2 NSs are intimately loaded on the surface of Bi_5O_7Br NSs. As shown in the HRTEM image of pure Bi_5O_7Br NSs (Fig. 1c), the lattice space distance of 0.245 nm is ascribed to (113) plane of Bi_5O_7Br [30]. As shown in Fig. 1d, the lattice with d space distances of 0.245 and 0.92 nm are attributed to the (113) plane of Bi_5O_7Br and the (002) plane of 1T-WS_2, indicating the coexistence of Bi_5O_7Br and 1T-WS_2. The above results prove the successful preparation of Bi_5O_7Br NSs and 1T-WS_2@Bi_5O_7Br-5 composites.

As shown in Fig. S5 (Supporting information), all catalysts display H3 hysteresis loops with type-IV isotherms, which is concordant with mesoporous of all samples [26]. The pore sizes of all samples are about 3–33 nm. As shown in Table S1 (Supporting

information), the specific surface areas of 1T-WS_2 NSs presents the smallest specific surface area (4.69 m^2/g). In addition, the specific surface areas of Bi_5O_7Br NSs, 1T-WS_2@Bi_5O_7Br-1, 1T-WS_2@Bi_5O_7Br-3, 1T-WS_2@Bi_5O_7Br-5 and 1T-WS_2@Bi_5O_7Br-7 composites are 63.44, 76.91, 35.94, 10.81 and 7.23 m^2/g, respectively. Surprisingly, the specific surface areas of 1T-WS_2@Bi_5O_7Br composites increase non-linearly with decreasing 1T-WS_2 NSs. When the 1T-WS_2 NSs loading amounts is 1%, the specific surface area of 1T-WS_2@Bi_5O_7Br composites is improved. Nevertheless, with the loading amount of 1T-WS_2 NSs increases from 3% to 7%, the specific surface area of 1T-WS_2@Bi_5O_7Br composites decreases. However, the photocatalytic performance of 1T-WS_2@Bi_5O_7Br-5 composites is the best, indicating that specific surface area is not the crucial factor in improving photocatalytic activity [32].

An absorption edge at ~500 nm is detected in Bi_5O_7Br NSs (Fig. 2a). Interestingly, the light absorption ability of 1T-WS_2@Bi_5O_7Br composites is better than Bi_5O_7Br NSs, and increases with the increase of 1T-WS_2 loading amount from 1% to 7%, consistent with the color modification from yellow to gray (Fig. S6 in Supporting information). This indicates that 1T-WS_2 NSs can effectively improve the light absorption ability of Bi_5O_7Br. The enhanced light absorption of 1T-WS_2@Bi_5O_7Br composite is beneficial for the production of electron-hole pairs [33]. Furthermore, the band gap energy (E_g) of all catalysts is calculated by $(\alpha h\nu)^{1/2} \propto h\nu - E_g$. Therefore, the band gaps of Bi_5O_7Br NSs, 1T-WS_2@Bi_5O_7Br-1, 1T-WS_2@Bi_5O_7Br-3, 1T-WS_2@Bi_5O_7Br-5 and 1T-WS_2@Bi_5O_7Br-7 composites are 2.25, 2.13, 2.00, 1.75 and 1.75 eV (Fig. 2b), respectively. Among them, both 1T-WS_2@Bi_5O_7Br-5 and 1T-WS_2@Bi_5O_7Br-7 composites present the narrowest band gap. Obviously, 1T-WS_2 loading can improve the light absorption of Bi_5O_7Br, which could improve the utilization of light and photocatalytic performance.

To further check the vital role of 1T-WS_2 in 1T-WS_2@Bi_5O_7Br composites, the photoexcited carrier lifetimes of pure Bi_5O_7Br NSs and 1T-WS_2@Bi_5O_7Br-5 composites are measured by the time-resolved PL spectroscopy. As shown in Fig. S7 (Supporting information), the intensity-average lifetime (τ) of 1T-WS_2@Bi_5O_7Br-5 composites (0.6907 ns) is longer than that of pure Bi_5O_7Br NSs (0.5208 ns), indicating that 1T phase WS_2 can efficiently capture photogenerated electrons of Bi_5O_7Br NSs and inhibit the recombination of electron-hole pairs [33].

To study the possibility of N_2 fixation, Mott-Schottky plots are tested to estimate the conduction band (CB) potential of pure Bi_5O_7Br and 1T-WS_2@Bi_5O_7Br composites. As exhibited in Fig. S8 (Supporting information), the flat band potentials (E_{FB}) of Bi_5O_7Br NSs and 1T-WS_2@Bi_5O_7Br-1, 1T-WS_2@Bi_5O_7Br-3, 1T-WS_2@Bi_5O_7Br-5 and 1T-WS_2@Bi_5O_7Br-7 composites are obtained and the results are −0.50, −0.53, −0.50, −0.65 and −0.55 eV *vs.* Ag/AgCl. The obtained E_{FB} is converted to a potential vs. standard hydrogen electrode (NHE), and then the value is subtracted by 0.2 eV to get a conduction band potential (E_{CB}) *vs.* NHE. Therefore, the E_{CB} of Bi_5O_7Br NSs, 1T-WS_2@Bi_5O_7Br-1, 1T-WS_2@Bi_5O_7Br-3, 1T-WS_2@Bi_5O_7Br-5 and 1T-WS_2@Bi_5O_7Br-7 composites are −0.48, −0.51, −0.48, −0.63 and −0.53 eV *vs.* NHE (Fig. 2c). Among these, the E_{CB} of 1T-WS_2@Bi_5O_7Br-5 composites is the most negative, indicating 1T-WS_2@Bi_5O_7Br-5 composites is more suitable for photocatalytic N_2 fixation.

Fig. 2d exhibits that all samples present the photocurrent responses on each illumination [33]. The photocurrent response curves of 1T-WS_2@Bi_5O_7Br composites (Fig. 2d) display higher current densities than pure Bi_5O_7Br NSs, indicating a noticeable improvement of carrier separation with 1T-WS_2 loading. First of all, the light absorption ability of 1T-WS_2@Bi_5O_7Br composites is higher than that of pure Bi_5O_7Br NSs, causing more photoexcited electron-hole pairs. Secondly, 1T phase WS_2 as an electron acceptor can accept photogenerated electrons, which can achieve more effective carrier separation. Among the 1T-WS_2@Bi_5O_7Br composites with different amounts of 1T-WS_2 NSs, 1T-WS_2@Bi_5O_7Br-5 composites present the highest current density. The charge transfers ability of pure Bi_5O_7Br NSs and 1T-WS_2@Bi_5O_7Br composites are further measured by EIS measurements [32,33]. Obviously, the 1T-WS_2@Bi_5O_7Br composites exhibit a smaller arc radius than that of pure Bi_5O_7Br NSs (Fig. 2e), illustrating that the 1T-WS_2 boosts the separation of carriers [33]. Besides, among the

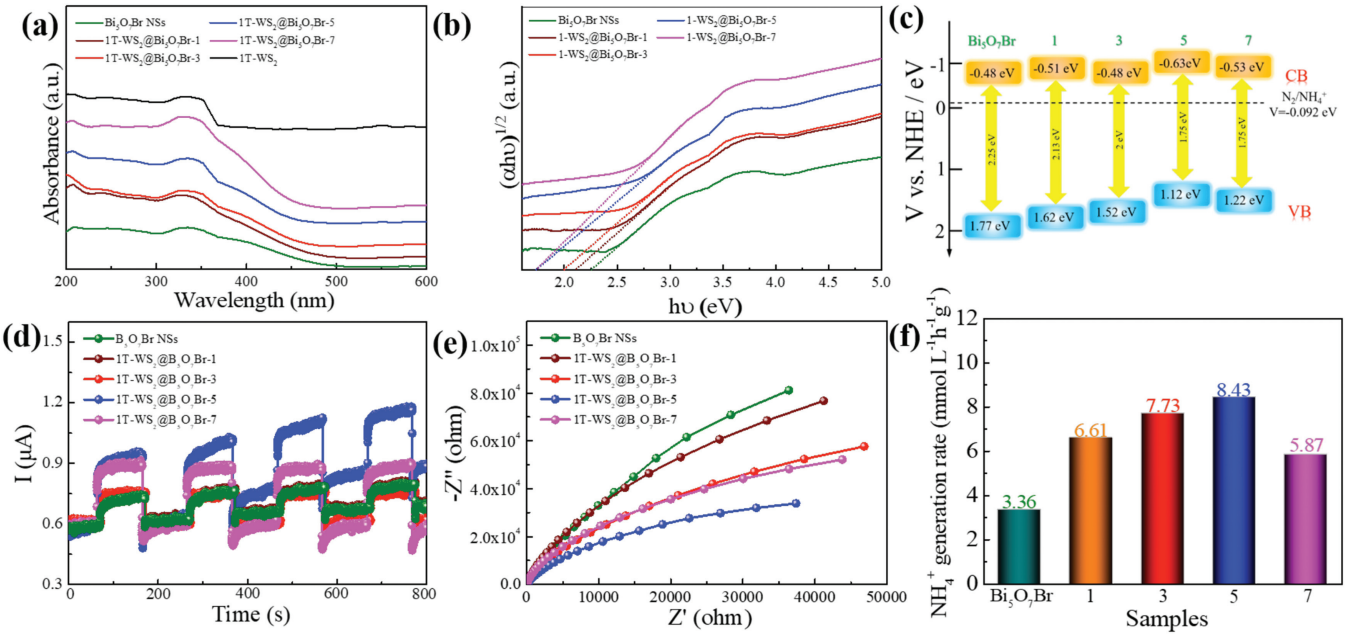

Fig. 2. (a) UV–vis absorption spectra, (b) band gap values, (c) schematic diagram of band gap, (d) the transient photocurrent responses, (e) EIS and (f) the NH_3 generation rates of Bi_5O_7Br NSs, 1T-WS_2 NSs and 1T-WS_2@Bi_5O_7Br composites.

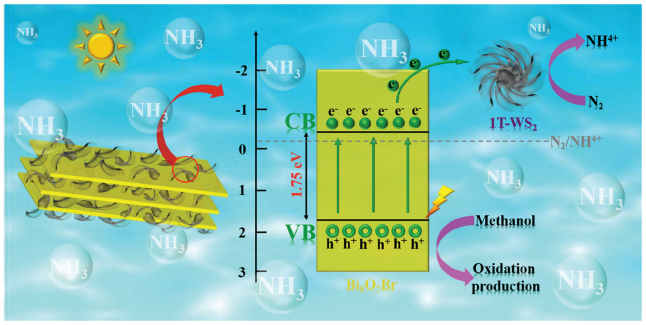

Scheme 2. The schematic illustration of photocatalytic mechanism of 1T-WS_2@Bi_5O_7Br composites.

1T-WS_2@Bi_5O_7Br composites with different amounts of 1T-WS_2 NSs, 1T-WS_2@Bi_5O_7Br-5 composites present the smallest arc radius, attributing to the best carrier separation efficiency. 1T phase WS_2 can enhance the carrier separation efficiency of Bi_5O_7Br, which can enhance the photocatalytic ability of Bi_5O_7Br.

The photocatalytic N_2 fixation performance of all samples is tested using the concentration of NH_4^+ under visible light illumination. The NH_3 generation rates of as-prepared samples are exhibited in Fig. 2f. The results indicate that the photocatalytic N_2 fixation activity of 1T-WS_2@Bi_5O_7Br composites is obviously better than that of pure Bi_5O_7Br NSs (3.36 mmol L^{-1} h^{-1} g^{-1}), which shows that the 1T phase WS_2 is beneficial to the enhancement of photocatalytic activity. It is worth mentioning that the photocatalytic activity of 1T-WS_2@Bi_5O_7Br composites enhances with increasing 1T-WS_2 amounts from 1% to 5% (Fig. 2f), owing to more effective carrier separation efficiency. However, further increasing 1T-WS_2 content from 5% to 7%, a decrease in photocatalytic activity is displayed, owing to the overmuch 1T-WS_2 loading on Bi_5O_7Br NSs hinders the photo-absorption of Bi_5O_7Br. 1T-WS_2@Bi_5O_7Br-5 composites exhibit the best photocatalytic N_2 fixation activity (8.43 mmol L^{-1} h^{-1} g^{-1}) because of the narrower band gap (Fig. 2b) and lower CB position (Fig. 2c). In order to evaluate the NH_4^+ production cycle property of 1T-WS_2@Bi_5O_7Br-5 composites, the photocatalytic N_2 fixation activity is measured for 9 h (Fig. S9 in Supporting information). Almost 88.4% of the incipient property is kept, showing satisfactory stability of 1T-WS_2@Bi_5O_7Br-5 composites. Furthermore, the XRD patterns of 1T-WS_2@Bi_5O_7Br-5 composites before and after cycle were detected. As shown in Fig. S10 Supporting information), F the position of the main characteristic peaks of 1T-WS_2@Bi_5O_7Br-5 composites do not change significantly, and the intensity of the characteristic peaks of Bi_5O_7Br is weakened due to the consumption of electrons. In addition, we compared photocatalytic activity for ammonia synthesis to previously reported catalysts (Table S2 in Supporting information), it is obvious that the photocatalytic performance of 1T-WS_2@Bi_5O_7Br-5 composite is excellent compared with the previous reports. The above results indicate that 1T-WS_2@Bi_5O_7Br-5 composites present excellent performance and stability for photocatalytic N_2 fixation.

According to the above experimental data, the photocatalytic mechanism of 1T-WS_2@Bi_5O_7Br composites is proposed (Scheme 2). Firstly, the 1T phase WS_2 decreases the E_g of Bi_5O_7Br (Fig. 2b), which improves light utilization to excite more photoelectrons. Secondly, the photogenerated electrons from Bi_5O_7Br NSs are quickly transferred to 1T phase WS_2 as electron acceptors, which can significantly enhance the efficiency of electron-hole separation. Then, 1T-WS_2 can provide active sites for N_2 activation to promote photocatalytic N_2 fixation. Usually, under solar light illumination, the photoelectrons of Bi_5O_7Br are excited and migrated to the surface of 1T phase WS_2 and reduce N_2 to NH_4^+. Simultaneously, the holes are consumed by methanol. Consequently, the close combination of 1T-WS_2 NSs and Bi_5O_7Br NSs significantly improves the photocatalytic N_2 fixation activity of 1T-WS_2@Bi_5O_7Br composites.

In conclusion, we report a photocatalyst that has excellent photocatalytic N_2 fixation performance by 1T-WS_2 NSs loading on Bi_5O_7Br NSs. Among prepared photocatalysts, the photocatalytic N_2 fixation rate of 1T-WS_2@Bi_5O_7Br-5 composites presents outstanding photocatalytic N_2 fixation activity (8.43 mmol L^{-1} h^{-1} g^{-1}), nearly 2.51 times higher than that of pure Bi_5O_7Br NSs. However, the excessive 1T-WS_2 NSs (7%) loading can hinder the absorption of light by Bi_5O_7Br, thereby reducing the photocatalytic performance of the catalyst. Therefore, 1T phase WS_2 cocatalyst is a promising substitute for the replacement of precious metals in photocatalysis to achieve the improved photocatalytic activity of B_5O_7Br NSs.

Declaration of competing interest

The authors report no declarations of interest.

Acknowledgments

The authors are thankful for funding from the National Natural Science Foundation of China (Nos. 51872173 and 51772176), Taishan Scholars Program of Shandong Province (No. tsqn201812068), Higher School Youth Innovation Team of Shandong Province (No. 2019KJA013), Science and Technology Special Project of Qingdao City (No. 20-3-4-3-nsh).

Appendix A. Supplementary data

Supplementary material related to this article can be found, in the online version, at doi:https://doi.org/10.1016/j.cclet.2021.03.077.

References

[1] X. Li, X. Sun, L. Zhang, et al., J. Mater. Chem. A 6 (2018) 3005–3011.
[2] J. Sun, W. Kong, Z. Jin, et al., Chin. Chem. Lett. 31 (2020) 953–960.
[3] B. Sun, P. Qiu, Z. Liang, et al., Chem. Eng. J. 406 (2021) 127177.
[4] W. Qiu, X. Xie, J. Qiu, et al., Nat. Commun. 9 (2018) 3485.
[5] G.N. Chrauzer, T.D. Guth, J. Am. Chem. Soc. 99 (1977) 7189–7193.
[6] J. Li, H. Li, G. Zhan, L. Zhang, Acc. Chem. Res. 50 (2017) 112–121.
[7] L. Chen, C. He, R. Wang, et al., Chin. Chem. Lett. 32 (2021) 53–56.
[8] C. Zhou, D. Huang, P. Xu, et al., Chem. Eng. J. 370 (2019) 1077–1086.
[9] K. Zhang, C. Liu, F. Huang, et al., Appl. Catal. B: Environ. 68 (2006) 125–129.
[10] F. Lei, Y. Sun, K. Liu, et al., J. Am. Chem. Soc. 136 (2014) 6826–6829.
[11] K. Zhao, L. Zhang, J. Wang, et al., J. Am. Chem. Soc. 135 (2013) 15750–15753.
[12] M. Guan, C. Xiao, J. Zhang, et al., J. Am. Chem. Soc. 135 (2013) 10411–10417.
[13] L. Ye, L. Zan, L. Tian, et al., Chem. Commun. 47 (2011) 6951–6953.
[14] H. Liu, Z. Fang, Y. Su, et al., Chem. Asian J. 7 (2018) 13.
[15] P. Li, Z. Zh, Q. Wang, M. Guo, J. Am. Chem. Soc. 142 (2020) 12430–12439.
[16] Q. Wang, X. Xue, Y. Lei, et al., Small 16 (2020) 202001571.
[17] L. Tang, Z. Lv, Y. Xue, et al., Chem. Eng. J. 374 (2019) 975–982.
[18] S. Han, L. Hu, Z. Liang, et al., Adv. Funct. Mater. 24 (2014) 5719–5727.
[19] Y. Liu, Q. Feng, W. Liu, et al., Nano Energy 81 (2021) 105641.
[20] R. Wei, Z. Huang, G. Gu, et al., Appl. Catal. B: Environ. 231 (2018) 101–107.
[21] D. Hadi, H. Aziz, S. Davod, A. Soheila, V. Elham, Ceram. Int. 45 (2019) 2542–2555.
[22] Y. Qin, C. Guo, Zh. Liang, et al., Chin. Chem. Lett. 32 (2021) 1524–1527.
[23] D. Wang, Y. Zou, L. Tao, et al., Chin. Chem. Lett. 30 (2019) 826–838.
[24] H. Xu, J. Yi, X. She, et al., Appl. Catal. B: Environ. 220 (2018) 379–385.
[25] H. Hao, X. Lang, ChemCatChem 11 (2019) 1378–1393.
[26] X. Dong, H. Hao, N. Wang, H. Yuan, X. Lang, J. Colloid Interface Sci. 590 (2021) 387–395.
[27] Q. Wang, Y. Lei, D. Wang, Y. Li, Energy Environ. Sci. 12 (2019) 1730–1750.
[28] Q. Wang, Y. Lei, Y. Wang, et al., Energy Environ. Sci. 13 (2020) 1593–1616.
[29] Y. Su, C. Ding, Y. Dang, et al., Appl. Surf. Sci. 346 (2015) 311–316.
[30] L. Zhang, X. Yue, J. Liu, et al., Sep. Purif. Technol. 231 (2020) 115917.
[31] J. Wu, Y. Xie, Y. Ling, Y. Dong, Front. Chem. 7 (2019) 649.
[32] X. Li, S. Lyu, X. Lang, Environ. Res. 195 (2021) 110851.
[33] Z. Liang, Y. Guo, Y. Xue, H. Cui, J. Tian, Nanoscale 11 (2019) 12266–12274.